

Chalcone Analogue as New Candidate for Selective Detection of α -Synuclein Pathology

Sho Kaide, Hiroyuki Watanabe, Shimpei Iikuni, Masato Hasegawa, Kyoko Itoh, and Masahiro Ono*

Cite This: <https://doi.org/10.1021/acchemneuro.1c00441>

Read Online

ACCESS |



Metrics & More



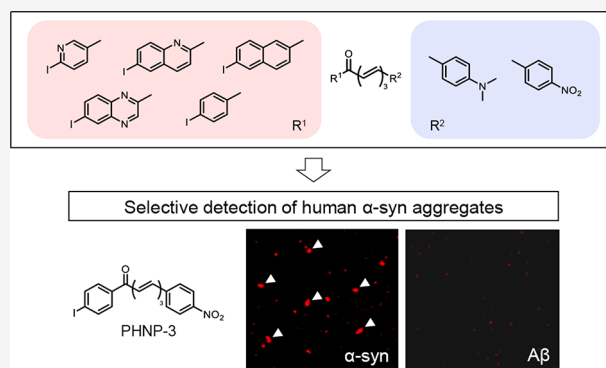
Article Recommendations



Supporting Information

ABSTRACT: Deposition of α -synuclein (α -syn) aggregates is one of the neuropathological hallmarks of synucleinopathies including Parkinson's disease, dementia with Lewy bodies, and multiple-system atrophy. In vivo detection of α -syn aggregates with SPECT or PET may be an effective tool for medical intervention against synucleinopathy. In the present study, we designed and synthesized a series of chalcone analogues with different aryl groups to evaluate their potential as α -syn imaging probes. In competitive inhibition assays, aryl groups markedly affected binding affinity and selectivity for recombinant α -syn aggregates. Chalcone analogues with a 4-(dimethylamino)phenyl group bound to both α -syn and amyloid β ($A\beta$) aggregates while ones with a 4-nitrophenyl group displayed α -syn-selective binding. In fluorescent staining, only chalcone analogues with a 4-nitrophenyl group succeeded in selective detection of human α -syn against $A\beta$ aggregates in patients' brain samples. Among them, PHNP-3 exhibited the most promising binding characteristics for α -syn aggregates ($K_i = 0.52$ nM), encouraging us to further evaluate its utility. Then, a ^{125}I -labeling reaction was performed to obtain [^{125}I]PHNP-3. In a binding saturation assay, [^{125}I]PHNP-3 bound to α -syn aggregates with high affinity ($K_d = 6.9$ nM) and selectivity. In a biodistribution study, [^{125}I]PHNP-3 exhibited modest uptake (0.78% ID/g at 2 min after intravenous injection) into a normal mouse brain. Although there is room for improvement of its pharmacokinetics in the brain, encouraging in vitro results in the present study indicate that further structural optimization based on PHNP-3 might lead to the development of a clinically useful probe targeting α -syn aggregates in the future.

KEYWORDS: chalcone analogue, 4-nitrophenyl group, imaging, α -synuclein



INTRODUCTION

Synucleinopathies such as Parkinson's disease (PD), dementia with Lewy bodies (DLB), and multiple-system atrophy (MSA) are neurodegenerative disorders characterized by abnormal deposition of Lewy bodies (LBs), Lewy neurites (LNs), and glial cytoplasmic inclusions (GCIs)^{1–4} that accumulate in the brain before the onset of the disease and propagate over time.^{5,6} PD and DLB patients show intraneuronal inclusions named LBs and LNs, which are mainly present in the substantia nigra, pons, and medulla oblongata. Contrary to inclusions found in PD and DLB, in MSA brains, GCIs are observed not only in neurons but also within oligodendrocytes. In addition to such different distributions between hallmarks, clinical symptoms of each synucleinopathy vary markedly.^{7,8}

α -Synuclein (α -syn) aggregates are major components of these typical pathological hallmarks and play a crucial role in disease progression of synucleinopathies. However, the pathological mechanisms of how α -syn aggregates cause neurodegeneration have not been clarified, suggesting that visualizing α -syn aggregates in the brain could be useful for early diagnosis, monitoring of disease progression, elucidation

of pathology, and developing therapeutic agents against synucleinopathy.^{9–11} In general, α -syn aggregates have abundant β -sheet structures as well as $A\beta$ aggregates, which are major biomarkers of Alzheimer's disease (AD). Both aggregates coexist in some synucleinopathy patients' brains,^{12,13} and the concentration of α -syn aggregates is much lower than that of $A\beta$ aggregates in diseased brains. Therefore, a tool for α -syn-selective recognition is critically needed for an accurate understanding of α -syn pathology in vivo to advance synucleinopathy research.¹⁴

Single-photon emission computed tomography (SPECT) and positron emission tomography (PET) are efficient nuclear molecular imaging techniques that enable real-time and noninvasive visualization with high sensitivity and quantifica-

Received: July 2, 2021

Accepted: December 1, 2021

tion. Over the past decade, significant progress has been made toward the development of nuclear medicine imaging probes targeting $A\beta$ and hyperphosphorylated tau aggregates in the AD patients, and some probes have been used in clinical stages.^{15,16} As with $A\beta$ and tau imaging, nuclear medicine imaging toward α -syn aggregates have attracted much attention, encouraging intensive research to develop α -syn-targeting probes.

Several nuclear medicine imaging probes targeting α -syn aggregates have been reported.¹⁴ A benzoxazole derivative ($[^{18}\text{F}]\text{BF227}$), phenothiazine-based ligands ($[^{11}\text{C}]\text{SIL5}$, $[^{125}\text{I}]\text{SIL23}$, and $[^{18}\text{F}]\text{SIL26}$), and a 3-(benzylidene)indolin-2-one-based ligand ($[^{18}\text{F}]\text{46a}$ or $[^{18}\text{F}]\text{WC58a}$) were proven to strongly bind to α -syn aggregates.^{17–22} However, they showed low binding selectivity for α -syn aggregates, low binding affinity for PD brain samples, or high nonspecific binding due to high lipophilicity, which made it difficult to clearly recognize α -syn pathology in vivo. These unfavorable properties limited further experiments to evaluate their potential as α -syn imaging probes. Recently, a benzoxazole-based ligand ($[^{18}\text{F}]\text{2FBox}$) and a phenyl isoxazole amide-based ligand ($[^{125}\text{I}]\text{61}$) were identified as hopeful candidates to develop α -syn-targeting probes using solid state NMR or cryo-electron microscopy structures of α -syn aggregates (Figure 1).^{23–28} Both probes

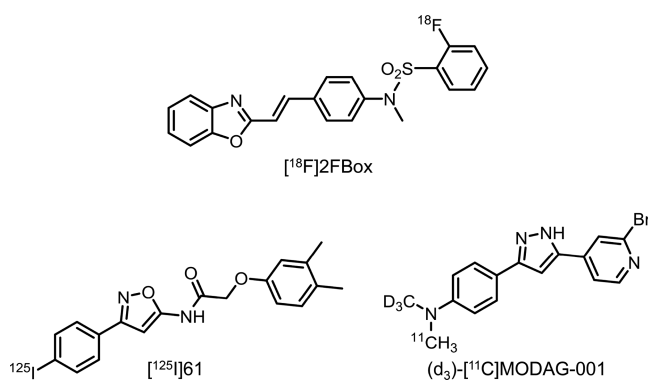


Figure 1. Chemical structures of α -syn imaging probes reported recently.

strongly bound to α -syn aggregates in vitro (dissociation constant $K_d = 1.1$ and 3.3 nM, respectively). In addition, $[^{18}\text{F}]\text{2FBox}$ displayed high α -syn-selectivity in vitro (over 30-fold selectivity versus $A\beta$ aggregates), and facilitated the recognition of α -syn aggregates in ex vivo autoradiography (ARG). However, it failed to identify α -syn aggregates in vivo in PET studies and in in vitro ARG studies using synucleinopathy brain sections.²⁷ A diarylpyrazole derivative ($(d_3)\text{-}[^{11}\text{C}]\text{MODAG-001}$) was designed based on an α -syn aggregation inhibitor to show high binding affinity ($K_d = 0.6$ nM) and selectivity for α -syn aggregates (over 30-fold selectivity versus $A\beta$ aggregates).²⁹ In addition, PET imaging with $(d_3)\text{-}[^{11}\text{C}]\text{MODAG-001}$ detected α -syn aggregates using α -syn-inoculated rats. However, nonspecific binding was also observed, preventing clear α -syn-detection in the rat brain. As described above, aggressive research on α -syn imaging has been conducted in the past decade; however, no probes have been studied clinically. Therefore, promising lead compounds for developing clinically useful nuclear medicine imaging probes toward α -syn aggregates are desired.

In parallel with research to develop feasible probes toward α -syn aggregates throughout the world, we have reported several

ligands such as benzimidazole derivatives, chalcone analogues, and bisquinoline derivatives as α -syn imaging probes.^{30–32} Among them, $[^{125}\text{I}]\text{IDP-3}$ bound to α -syn aggregates with high binding affinity (inhibition constant $K_i = 1.7$ nM), allowing it to effectively recognize α -syn aggregates in a synucleinopathy brain section (Figure 2).³² In addition, the chalcone structure has been widely used throughout the world to create imaging or therapeutic agents targeting β -sheet structures.^{23,33}

Therefore, we hypothesized that chalcone analogues such as IDP-3 might function as hopeful candidates for in vivo detection of α -syn pathology. We previously reported that aryl groups introduced into a chalcone structure might affect binding affinity for $A\beta$ aggregates.³⁴ These findings suggested that chalcone analogues with appropriate aryl groups may exhibit selective binding to α -syn against $A\beta$ aggregates, which prompted us to change an aryl group at the R^1 position of IDP-3. Furthermore, we focused on the structure–activity relationship studies on phenothiazine-based and 3-(benzylidene)indolin-2-one-based ligands previously reported.^{18–21} We found that the introduction of a nitro group improved the binding selectivity toward α -syn against $A\beta$ aggregates. This encouraged us to convert a (dimethylamino)phenyl group at the R^2 position of chalcone analogues into a nitrophenyl group for the improvement of α -syn selectivity. In the present study, we designed a series of chalcone analogues with a variety of aryl groups at R^1 and R^2 positions, aiming for α -syn imaging in vivo with high binding affinity and selectivity (Figure 2). Then, we synthesized them to evaluate their usefulness as α -syn-targeting probes.

RESULTS AND DISCUSSION

Chemistry. The synthetic route of chalcone analogues was shown in Scheme 1. The starting materials (**1**, **4**, **9**, **13**, and **19**) and 4-iodoacetophenone were commercially available products. 4-Iodoaryl ethanones (**3**, **8**, **12**, and **18**) were synthesized by the exchange reaction of bromine to tributyltin and tributyltin to iodine with or without the oxidation of a methyl group and subsequent Henry reaction. 3-(4-Nitrophenyl) prop-2-enal (**20**) and 5-(4-nitrophenyl)penta-2,4-dienal (**21**) were synthesized by the Wittig reaction, which was previously used to obtain 5-(4-dimethylaminophenyl)penta-2,4-dienal.³⁰ Then, the Claisen–Schmidt condensation reaction was performed between 4-iodoaryl ethanones and 5-aryl-penta-2,4-dienals to obtain final compounds (**22–30**) with total yields of 1.3–39%. The precursor of the ^{125}I -labeling reaction (**32**) was obtained from a corresponding bromo compound (**31**).

Competitive Inhibition Assay. A competitive inhibition assay was conducted to determine the binding affinity of chalcone analogues toward α -syn aggregates (Table 1). Thioflavin T (ThT) was used as a competitive ligand because it is one of the fluorescent dyes that can increase fluorescent intensity when it becomes attached to β -sheet structures in amyloid protein aggregates,³⁵ and ThT-competitive binding assays have been generally applied for developing α -syn- or $A\beta$ -targeting probes. Chalcone analogues with an iodo-pyridyl, iodoquinolyl, iodonaphthyl, or iodoquinolalanyl group at the R^1 position and a 4-(dimethylamino)phenyl group at the R^2 position (PYDP-3, QLDP-3, NPDP-3, and QXDP-3) competed well with ThT on α -syn aggregates to show preferable K_i values for α -syn aggregates (0.49–0.68 nM). These results indicated that our chalcone analogues showed lower binding affinity than phenothiazine derivatives (K_i values were 32.1, 57.9, and 49.0 nM for SIL5, SIL23, and SIL26, respectively),¹⁸

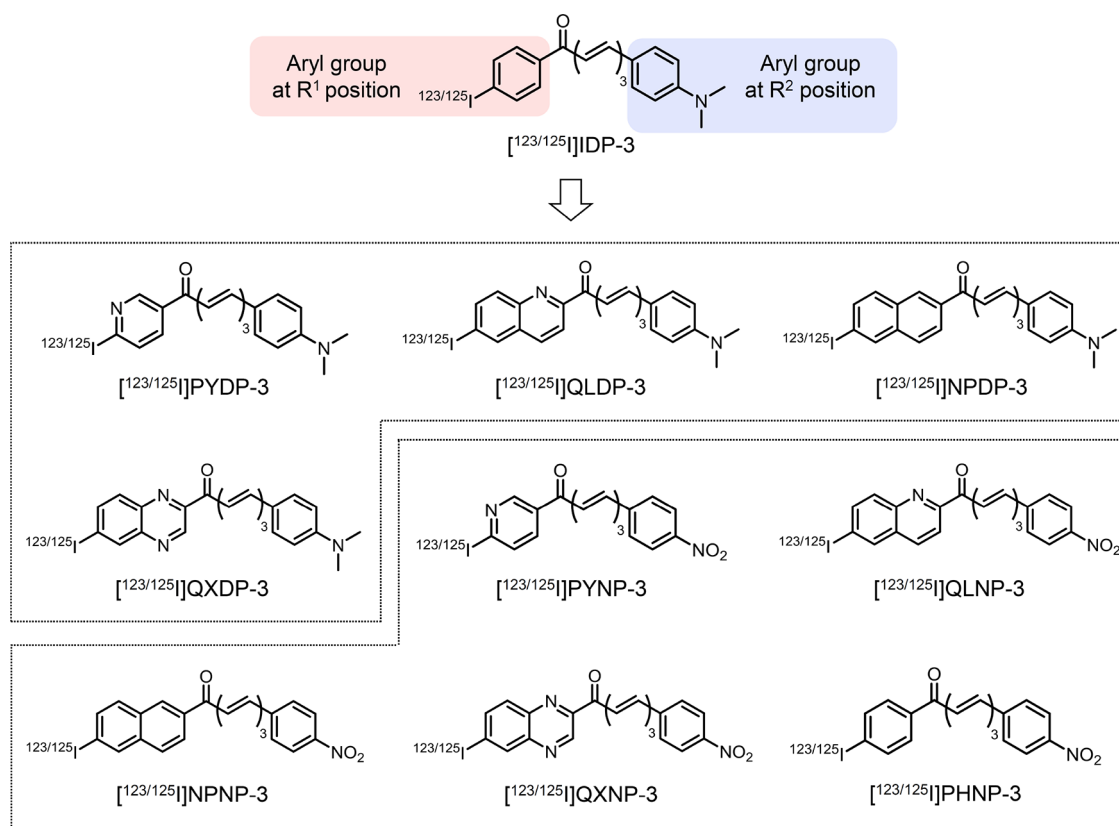


Figure 2. Chemical structure of $[^{123/125}\text{I}]$ IDP-3 and designs of $^{123/125}\text{I}$ -labeled chalcone analogues in the present study.

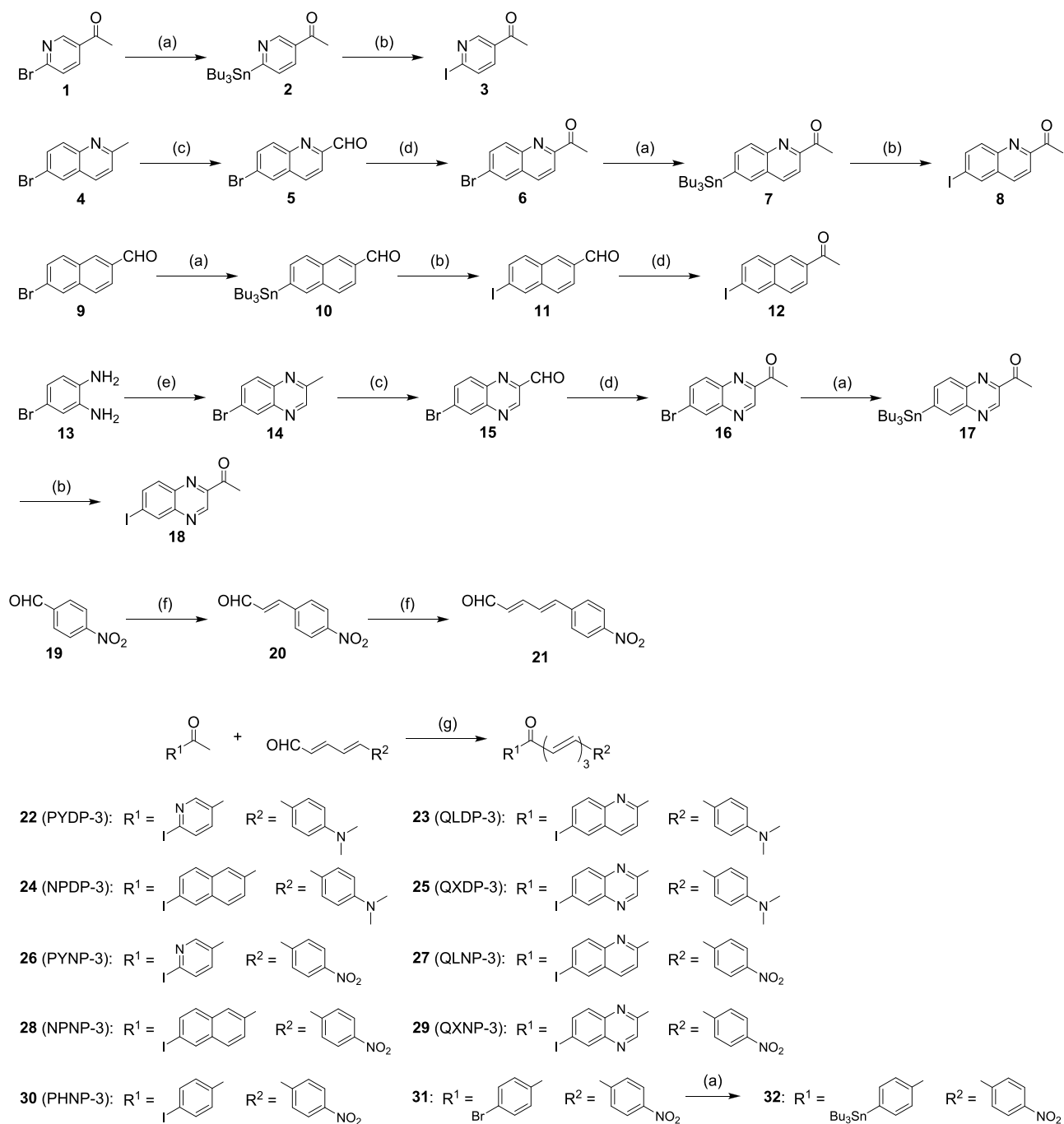
a 3-(benzylidene)indolin-2-one derivative (2.1 nM for compound **46a**),²¹ and IDP-3 (1.7 nM).³² Although comparisons of K_i values need to be interpreted carefully because assay protocols are different between groups, these chalcone analogues were suggested to represent higher binding affinity toward α -syn aggregates than reported α -syn-targeting probes. In order to clearly recognize α -syn pathology in vivo, selective binding to α -syn against $A\beta$ aggregates is also required for α -syn imaging probes. Thus, we estimated binding affinity of chalcone analogues with a 4-(dimethylamino)phenyl group for $A\beta$ aggregates. They also competed well with ThT on $A\beta$ aggregates to show a wide range of K_i values for $A\beta$ aggregates (1.1–25 nM), which led to a variety of ratios of K_i values for α -syn versus $A\beta$ aggregates (2.2–42). These results suggest that aryl groups at the R^1 position of chalcone analogues might affect binding selectivity for α -syn aggregates by changing binding affinity for $A\beta$ aggregates, which correlated with findings in our previous study on developing $A\beta$ -targeting probes based on the chalcone structure.³⁶

Next, binding characteristics of chalcone analogues with an iodopyridinyl, iodoquinolinyl, iodonaphthyl, iodoquinoxalyl, or iodophenyl group at the R^1 position and a 4-nitrophenyl group at the R^2 position (PYNP-3, QLNP-3, NPNP-3, QXNP-3, and PHNP-3) were evaluated in the same way. They competed well with ThT as well as chalcone analogues with a 4-(dimethylamino)phenyl group to display a variety of K_i values for α -syn aggregates (0.52–13 nM), which depended on the kinds of aryl groups at the R^1 position. Among them, PHNP-3 exhibited the most preferable binding affinity ($K_i = 0.52$ nM). Then, binding affinity for $A\beta$ aggregates was also evaluated. To our surprise, these analogues did not markedly compete with ThT on $A\beta$ aggregates; therefore, their K_i values for $A\beta$

aggregates could not be determined. These observations suggested that a 4-nitrophenyl group introduced into the R^2 position of chalcone analogues might markedly contribute to selective binding to α -syn against $A\beta$ aggregates.

In this experiment, it was suggested that aryl groups introduced into the R^1 and R^2 positions in chalcone analogues might affect binding affinity and selectivity for α -syn aggregates. In particular, the introduction of a nitrophenyl group at the R^2 position might be a key factor for leading to the high-level binding selectivity of α -syn for $A\beta$ aggregates. Considering that some α -syn imaging probes reported previously have a nitrophenyl group while few $A\beta$ imaging probes have one, such discussion may be reasonable although details remain unclear.

Fluorescent Staining. Fluorescent staining with chalcone analogues of paraffin-embedded synucleinopathy brain sections was carried out in order to evaluate the binding affinity for not only recombinant but also human α -syn aggregates. Several fluorescent spots of PYDP-3, QLDP-3, NPDP-3, and QXDP-3 were observed in synucleinopathy brain sections (Figure 3A,C,E,G). The localization of their fluorescent spots matched with that of positive spots on immunohistochemical staining using an anti- α -syn antibody, respectively (Figure 3B,D,F,H), which indicated that these chalcone analogues clearly stained human α -syn aggregates in the synucleinopathy brain. These results were correlated with that of competitive inhibition assay, which showed high binding affinity toward α -syn aggregates. As in the competitive inhibition experiment, binding affinities of PYDP-3, QLDP-3, NPDP-3, and QXDP-3 for $A\beta$ aggregates in the AD brain were also evaluated. As observed in α -syn staining with the synucleinopathy brain sections, fluorescent spots of each chalcone analogue (Figure

Scheme 1. Synthetic Route of Chalcone Analogues^a

^aReagents and conditions: (a) $(\text{Bu}_3\text{Sn})_2$, $\text{Pd}(\text{PPh}_3)_4$, dioxane, Et_3N , reflux, $95\text{ }^\circ\text{C}$; (b) I_2 , CHCl_3 , rt; (c) SeO_2 , dioxane, reflux, $100\text{ }^\circ\text{C}$; (d) nitromethane, 1,1,3,3-tetramethylguanidine, toluene, $110\text{ }^\circ\text{C}$; (e) methylglyoxal (40% in H_2O), EtOH , reflux, $50\text{ }^\circ\text{C}$; (f) (1) (1,3-dioxolan-2-yl)methyltriphenylphosphonium bromide, 18-crown-6, NaH , THF , rt, (2) 6 N HCl aq, THF , rt; (g) 10% KOH , EtOH , DMF , rt.

3I,K,M,O) were consistent with those of immunohistochemical staining with an anti- $\text{A}\beta$ antibody (Figure 3J,L,N,P). These observations indicated that chalcone analogues with a 4-(dimethylamino)phenyl group led to the clear visualization of AD-derived $\text{A}\beta$ aggregates, which is reasonable because they bound to synthetic $\text{A}\beta$ aggregates with high or moderate binding affinities in the competitive inhibition assay.

Then, the binding characteristics of PYNP-3, QLNP-3, NPNP-3, QXNP-3, and PHNP-3 were evaluated. Taking into consideration that strong fluorescent spots of each chalcone analogue (Figure 4A,C,E,G,I) corresponded to positive sites in

immunohistochemical staining of the same sections (Figure 4B,D,F,H,J), these chalcone analogues successfully recognized human α -syn aggregates as well as analogues with a 4-(dimethylamino)phenyl group. However, in the case of AD brain sections, strong fluorescent spots of these analogues were not detected (Figure 4K,M,O,Q,S) in $\text{A}\beta$ -positive regions on immunohistochemical staining (Figure 4L,N,P,R,T), suggesting that chalcone analogues with a 4-nitrophenyl group did not markedly bind to human $\text{A}\beta$ aggregates. On the other hand, weak fluorescent spots of each chalcone analogue were also observed in the fluorescent staining of both synucleinopathy

Table 1. K_i Values of Chalcone Analogues for α -Syn and $A\beta$ Aggregates ($n = 3$)^a and their K_i Ratios

Compound	R ¹	R ²	α -syn (nM)	$A\beta$ (nM)	K_i ratio ($A\beta/\alpha$ -syn)
PYDP-3			0.49 ± 0.13	1.1 ± 0.66	2.2
QLDP-3			0.52 ± 0.08	5.5 ± 3.2	11
NPDP-3			0.68 ± 0.15	9.9 ± 7.2	15
QXDP-3			0.59 ± 0.07	25 ± 16	42
PYNP-3			0.84 ± 0.05	n.d.	n.d.
QLNP-3			13 ± 1.6	n.d.	n.d.
NPNP-3			5.4 ± 0.63	n.d.	n.d.
QXNP-3			2.9 ± 0.18	n.d.	n.d.
PHNP-3			0.52 ± 0.06	n.d.	n.d.

^aEach value represents the mean \pm SD.

and AD brain sections. However, the localization of these weak signals did not match with that of positive spots in the immunohistochemical staining with anti- α -syn and anti- $A\beta$ antibodies, indicating that these weak signals were derived from the nonspecific binding of our chalcone analogues with high lipophilicity. In this experiment, PYNP-3, QLNP-3, NPNP-3, QXNP-3, and PHNP-3 clearly detected not human $A\beta$ but human α -syn aggregates, which was also correlated with results of the competitive inhibition assay using recombinant or synthetic protein aggregates. Human tau binding was not markedly observed (Figure S1). Other groups recently performed fluorescent staining with their original probes targeting α -syn aggregates by similar methods.^{37,38} This is the first report on α -syn imaging probes that successfully and selectively recognized human α -syn against $A\beta$ aggregates. These findings indicate that chalcone analogues with a 4-nitrophenyl group might function as useful α -syn imaging probes from the viewpoint of binding characteristics in the human brain as well as promising probes reported by other groups.

In the in vitro experiments using recombinant proteins or human brain samples, PHNP-3 displayed the most promising binding characteristics such as marked binding affinity and selectivity for recombinant and human α -syn aggregates, leading to further evaluation of this analogue.

¹²⁵I-Labeling. We performed an ¹²⁵I-labeling reaction of PHNP-3 from a corresponding tributyltin precursor by iododestannylation reaction with hydrochloric acid and hydrogen peroxide (Scheme 2). We identified [¹²⁵I]PHNP-3 by a comparison of retention time with nonradioactive PHNP-3 in reverse-phase high-performance liquid chromatography (HPLC). After a ¹²⁵I-labeling reaction, HPLC-purified [¹²⁵I]PHNP-3 exhibited greater than 95% radiochemical purity with 25% radiochemical yield.

Binding Saturation Assay. In order to further confirm the binding affinity of PHNP-3, the binding saturation assay was carried out to directly measure the binding affinity of [¹²⁵I]PHNP-3 for α -syn aggregates. In this experiment, [¹²⁵I]PHNP-3 exhibited specific binding toward α -syn aggregates at a K_d value of 6.9 ± 2.3 nM and maximum

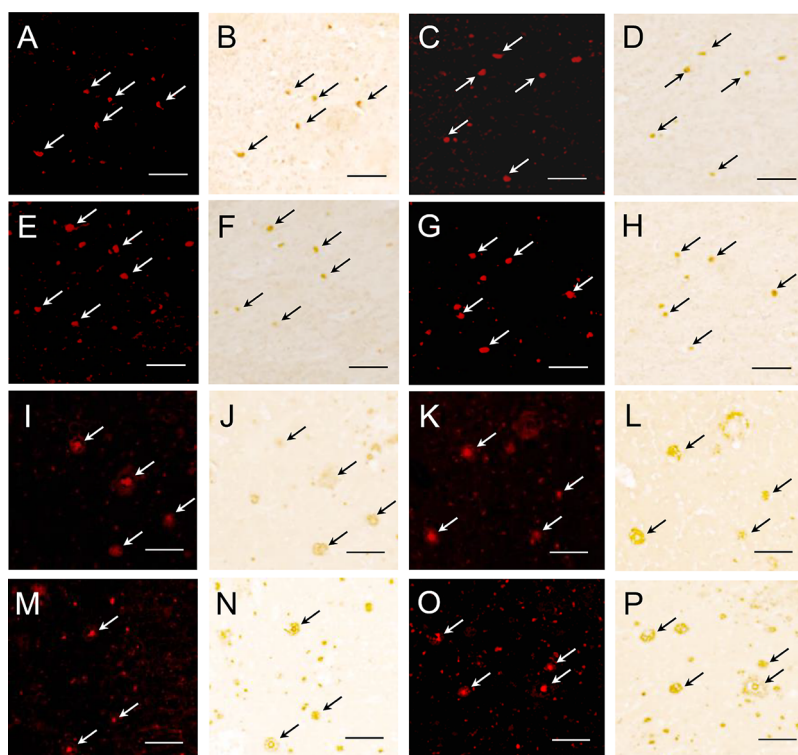


Figure 3. Fluorescence staining of PYDP-3, QLDP-3, NPDP-3, and QXDP-3 in basal ganglia sections from a synucleinopathy patient (A, C, E, and G, respectively) or frontal lobe sections from an AD patient (I, K, M, and O, respectively). Immunohistochemical staining of the same sections for (A), (C), (E), (G), (I), (K), (M), and (O) with an antibody against α -syn (B, D, F, and H, respectively) or A β (J, L, N, and P, respectively). Scale bars, 100 μ m.

number of binding sites (B_{\max}) of 9.5 ± 3.5 pmol/nmol protein (Figure S2A). The binding affinity of [125 I]PHNP-3 for A β aggregates was also determined, revealing that the K_d value and B_{\max} were 102 ± 21 nM and 57.6 ± 7.7 pmol/nmol protein, respectively (Figure S2B). These results suggest that [125 I]PHNP-3 displays high affinity and selectivity for α -syn against A β aggregates, reflecting the results of inhibition assays using recombinant proteins or human brain sections. Moreover, [125 I]PHNP-3 showed as high affinity toward α -syn aggregates as reported probes ($K_d = 8.9$ nM for [18 F]46a, 3.3 nM for [18 F]2FBox, and 1.1 nM for [125 I]61).^{21,27,28} Although [125 I]PHNP-3 detected fewer binding sites (B_{\max}) on α -syn compared with A β aggregates, its appropriate K_d values suggested that [125 I]PHNP-3 might be a promising candidate for in vivo α -syn imaging.

Stability Analysis in Murine Plasma. In order to determine the in vitro stability of [125 I]PHNP-3, it was incubated in murine plasma for 1 h at 37 °C. In the HPLC analysis after incubation, the radioactivity peak after 1 h incubation showed no change in comparison with that before incubation (Figure S3). This result suggests that [125 I]PHNP-3 is highly stable in murine plasma, which encouraged us to conduct further in vivo evaluation of this analogue.

Biodistribution Study. In order to evaluate the in vivo pharmacokinetics of [125 I]PHNP-3 in the brain, a biodistribution study with normal mice was carried out (Table 2). [125 I]PHNP-3 did not display sufficient brain uptake, 0.78% injected dose/gram (% ID/g) at 2 min after intravenous injection, to achieve α -syn imaging in vivo. However, high radioactivity accumulation was observed in the blood. These results may be explained by high lipophilicity of [125 I]PHNP-3 (clog = 5.62) to bind to plasma proteins, which might prevent

its blood–brain barrier (BBB) penetration.³⁹ Besides its high lipophilicity, the relatively larger molecular weight (431 Da) and size of [125 I]PHNP-3 compared with clinically used A β and tau imaging probes, as well as its substrate capacity for transporters overexpressed at BBB, may also be important factors explaining the weak capacity to penetrate BBB. To date, α -syn imaging studies have not progressed to the clinical phase; however, similar criteria to those for A β and tau imaging in vivo need to be applied for in vivo α -syn imaging, indicating that α -syn-targeting probes need to exhibit high initial uptake ($\geq 4\%$ ID/g at 2 min after intravenous injection) into and rapid clearance ($\leq 1\%$ ID/g at 30 min after intravenous injection) from the mouse brain.^{40,41} Although [125 I]PHNP-3 did not satisfy these requirements, it displayed equal or higher brain uptake than [18 F]2FBox (0.47% ID/g peak at 12 min after intravenous injection), which detected α -syn aggregates in an ex vivo ARG study.²⁷ Taking into consideration that [125 I]PHNP-3 showed as high binding affinity as [18 F]2FBox ($K_d = 5.8$ and 3.3 nM, respectively)²⁷ and preferable selectivity toward α -syn aggregates in vitro, [125 I]PHNP-3 may be useful as a lead compound for the development of α -syn-targeting probes in the future.

The distribution of radioactivity throughout the body was also determined. [125 I]PHNP-3 initially showed high accumulation in the liver (16.4% ID/g at 2 min after intravenous injection) and thereafter in the intestine (3.86% ID/g at 60 min after intravenous injection). The radioactivity accumulation in the thyroid was negligible (0.08% ID at 60 min after intravenous injection), indicating that [125 I]PHNP-3 showed no marked deiodination in vivo by 60 min post injection.

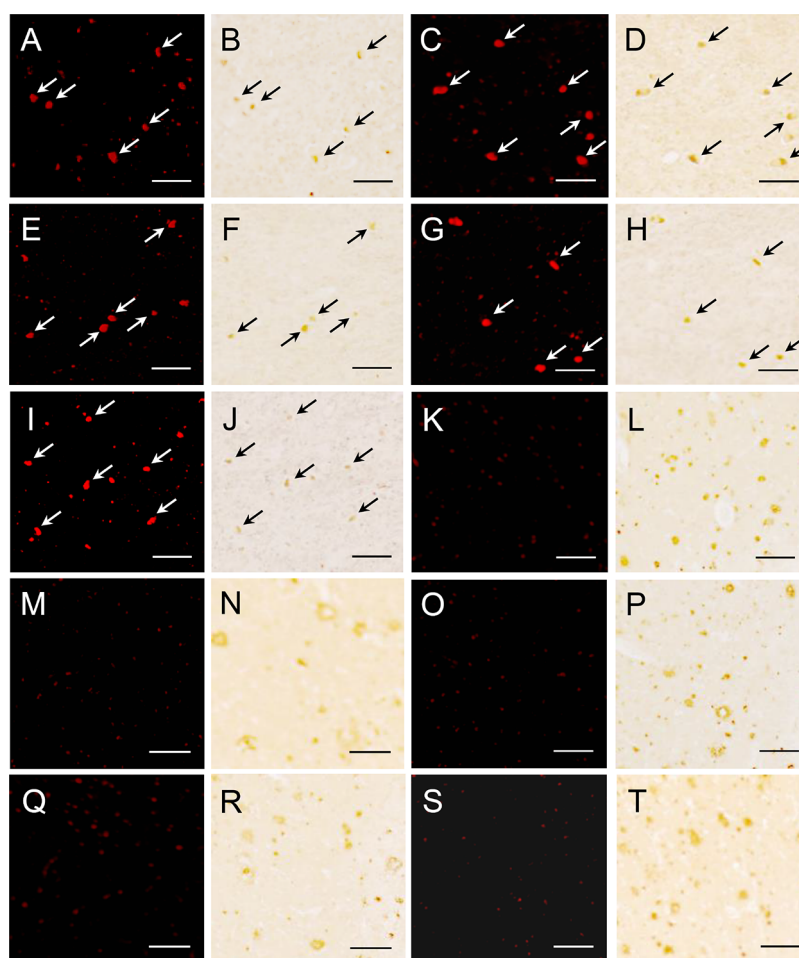
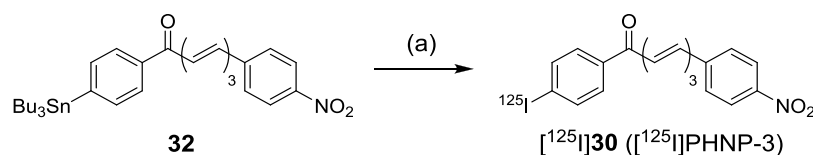


Figure 4. Fluorescence staining of PYNP-3, QLNP-3, NPNP-3, QXNP-3, and PHNP-3 in basal ganglia sections from a synucleinopathy patient (A, C, E, G, and I, respectively) or frontal lobe sections from an AD patient (K, M, O, Q, and S, respectively). Immunohistochemical staining of the same sections for (A), (C), (E), (G), and (I) with an antibody against α -syn (B, D, F, H, and J, respectively) or $A\beta$ (L, N, P, R, and T, respectively). Scale bars, 100 μ m.

Scheme 2. ^{125}I -Labeling Reaction of PHNP-3 by Iododestannylation Reaction^a



^aReagents and conditions: (a) [^{125}I]NaI, 3% H_2O_2 , 1 N HCl aq, EtOH, DMF, 80 $^\circ\text{C}$.

CONCLUSIONS

We designed and synthesized novel chalcone analogues to evaluate their potential as nuclear medicine imaging probes for α -syn detection in vivo. In a competitive inhibition assay, aryl groups introduced into the R^1 and R^2 positions in chalcone analogues affected binding affinity and selectivity toward α -syn aggregates. Chalcone analogues with a 4-(dimethylamino)-phenyl group at the R^2 position recognized both α -syn and $A\beta$ aggregates, whereas those with a 4-nitrophenyl group detected α -syn aggregates with high affinity and selectivity. In the fluorescent staining, only chalcone analogues with a 4-nitrophenyl group successfully exhibited selective detection of human α -syn against $A\beta$ aggregates. Among them, PHNP-3 especially displayed preferable binding characteristics toward α -syn aggregates, encouraging us to obtain [^{125}I]PHNP-3 by

^{125}I -labeling reaction. In a binding saturation assay, [^{125}I]PHNP-3 displayed high binding affinity and selectivity toward α -syn aggregates. In a biodistribution study, [^{125}I]PHNP-3 was moderately permeable to BBB, which should be overcome to achieve clear recognition of α -syn aggregates in vivo. However, promising in vitro properties of [^{125}I]PHNP-3 suggested that it might function as a new candidate for developing clinically promising α -syn-targeting probes. Further structural activity relationship studies based on [^{125}I]PHNP-3 aiming for improving brain uptake while maintaining its preferable binding characteristics for α -syn aggregates may lead to selective detection of α -syn pathology in vivo. Such examination is ongoing.

Table 2. Radioactivity Accumulation after Intravenous Injection of [¹²⁵I]PHNP-3 in Normal Mice (Male, *n* = 5)^a

tissue	time after injection (min)			
	2	10	30	60
blood	28.9 (2.52)	20.4 (1.58)	15.1 (2.19)	12.4 (1.60)
spleen	4.73 (0.71)	4.48 (0.48)	4.51 (0.53)	4.81 (0.81)
pancreas	2.01 (0.45)	2.31 (0.31)	2.00 (0.27)	1.85 (0.28)
stomach ^b	0.57 (0.14)	0.70 (0.17)	1.04 (0.57)	1.01 (0.49)
intestine	0.93 (0.08)	1.56 (0.28)	2.45 (0.48)	3.86 (0.51)
kidney	6.94 (0.52)	5.89 (0.24)	4.65 (0.67)	4.56 (0.64)
liver	16.4 (8.15)	15.5 (1.31)	12.5 (1.43)	11.5 (1.34)
heart	8.72 (1.29)	6.41 (0.50)	4.61 (0.48)	3.87 (0.75)
lung	17.2 (0.82)	11.3 (0.93)	9.21 (0.30)	7.95 (1.82)
brain	0.78 (0.03)	0.74 (0.08)	0.73 (0.11)	0.61 (0.11)
thyroid ^b	0.07 (0.03)	0.07 (0.03)	0.08 (0.02)	0.08 (0.02)

^aExpressed as % injected dose per gram. Each value represents the mean (SD). ^bExpressed as % injected dose.

METHODS

General Remarks. Reagents purchased from commercial sources were used without further purification. Purification of crude compounds were performed by Smart Flash EPCLC W-Prep 2XY (Yamazen Corporation, Osaka, Japan). ¹H NMR spectra were obtained by JEOL JNM-ECS400 (JEOL, Tokyo, Japan) using tetramethylsilane as an internal standard. Chemical shift (δ) and coupling constants (*J*) are recorded as ppm and hertz (Hz), respectively. The multiplicity is recorded by singlet (s), doublet (d), double doublet (dd), double double doublet (ddd), quartet (q), or multiplet (m). ESI and EI mass spectrometry were performed with a Shimadzu LCMS-2020 (Shimadzu, Kyoto, Japan) and a Shimadzu GCMS-QP2010 PL (Shimadzu). HPLC analysis was performed on a Shimadzu system (an LC-20 AD pump with an SPD-20A UV detector). The samples were analyzed by a Cosmosil C₁₈ column (SC₁₈-MS-II 4.6 mm ID \times 150 mm; Nacalai Tesque, Kyoto, Japan), which was eluted with an isocratic system at a flow rate of 1.0 mL/min. Acetonitrile/H₂O was used as the mobile phase to prove that all key compounds showed over 95% purity. Animal experiments were conducted in accordance with the ethical guidelines of the Kyoto University animal experimentation committee. ddY mice were purchased from Japan SLC, Inc. (Shizuoka, Japan) and given ad libitum access to water and food. Experiments with human brain samples were conducted in accordance with the ethical guidelines of the Ethics Committee of Kyoto Prefectural University of Medicine. Informed consent was secured from all patients.

Chemistry. **5-Acetyl-2-(tributylstannyl)pyridine (2).** A mixture of **1** (200 mg, 1.00 mmol), bis(tributyltin) (3 mL, 12.0 mmol), and Pd(PPh₃)₄ (231 mg, 0.20 mmol) in a mixed solvent (15 mL, dioxane/Et₃N = 2/1) was stirred at 95 °C under reflux for 2.5 h. The solvent was removed, and the residue was purified by silica gel chromatography (ethyl acetate/hexane = 1/4) to give **2** (120 mg, 29.3%). ¹H NMR (400 MHz, CDCl₃) δ 8.92 (d, *J* = 2.0 Hz, 1H), 7.84 (d, *J* = 8.8 Hz, 1H), 7.72 (dd, *J* = 1.6, 8.0 Hz, 1H), 2.58 (s, 3H), 1.86–1.66 (m, 6H), 1.54–1.42 (m, 6H), 1.35–1.18 (m, 6H), 0.94–0.88 (m, 9H). MS (ESI) *m/z* 412.2 [M+H]⁺.

5-Acetyl-2-iodopyridine (3). A mixture of **2** (120 mg, 0.29 mmol) and iodine (3.3 mg, 0.013 mmol) in chloroform (5 mL) was stirred at room temperature (rt) for 30 min. Saturated NaHSO₃ aq was added to quench the reaction. The mixture was extracted with chloroform after neutralization with saturated NaHCO₃ aq, and the combined organic layer was dried over Na₂SO₄, concentrated, and purified by silica gel chromatography (ethyl acetate/hexane = 1/4) to give **3** (45.7 mg, 63.2%). ¹H NMR (400 MHz, CDCl₃) δ 8.87 (d, *J* = 2.4 Hz, 1H), 7.88 (d, *J* = 8.4 Hz, 1H), 7.83 (dd, *J* = 2.4, 8.4 Hz, 1H), 2.61 (s, 3H). MS (ESI) *m/z* 247.9 [M+H]⁺.

6-Bromoquinoline-2-carboxaldehyde (5). To a solution of **4** (444 mg, 2.0 mmol) in dioxane (20 mL) was added SeO₂ (266 mg, 2.4

mmol). The mixture was stirred at 100 °C under reflux for 13 h. The mixture was extracted with chloroform, and the combined organic layer was dried over Na₂SO₄, concentrated, and purified by silica gel chromatography (ethyl acetate/hexane = 1/3) to give 286 mg of **5** (60.9%). ¹H NMR (400 MHz, CDCl₃) δ 10.2 (s, 1H), 8.23 (d, *J* = 8.4 Hz, 1H), 8.13 (d, *J* = 8.8 Hz, 1H), 8.09 (d, *J* = 2.0 Hz, 1H), 8.05 (d, *J* = 8.4 Hz, 1H), 7.90 (dd, *J* = 2.4, 8.8 Hz, 1H). MS (ESI) *m/z* 236.0 [M+H]⁺.

1-(6-Bromoquinoline-2-yl)ethanone (6). To a solution of **5** (200 mg, 0.85 mmol) in toluene (636 μ L) were added nitromethane (206 μ L, 3.81 mmol) and 1,1,3,3-tetramethyl guanidine (16.1 μ L, 0.13 mmol). The mixture was stirred at 110 °C for 1.5 h. Saturated NaHCO₃ aq was added to quench the reaction. The mixture was extracted with ethyl acetate, and the combined organic layer was dried over Na₂SO₄, concentrated, and purified by silica gel chromatography (ethyl acetate/hexane = 1/6) to give 83.0 mg of **6** (39.2%). ¹H NMR (400 MHz, CDCl₃) δ 8.16 (q, *J* = 7.7 Hz, 2H), 8.07 (d, *J* = 9.2 Hz, 1H), 8.05 (d, *J* = 2.0 Hz, 1H), 7.85 (dd, *J* = 2.0, 8.8 Hz, 1H), 2.86 (s, 3H). MS (ESI) *m/z* 250.0 [M+H]⁺.

1-(6-(Tributylstannyl)quinoline-2-yl)ethanone (7). Compound **7** was synthesized from **6** according to the method described above to prepare **3** (25 mg, 48.6%). ¹H NMR (400 MHz, CDCl₃) δ 8.24 (s, 1H), 8.08 (d, *J* = 1.2 Hz, 2H), 7.94 (d, *J* = 2.0 Hz, 1H), 7.90 (d, *J* = 8.4 Hz, 1H), 2.87 (s, 3H), 1.68–1.54 (m, 6H), 1.48–1.36 (m, 6H), 1.28–1.18 (m, 6H), 0.91–0.88 (m, 9H). MS (ESI) *m/z* 462.3 [M+H]⁺.

1-(6-Iodoquinoline-2-yl)ethanone (8). Compound **8** was synthesized from **7** according to the method described above to prepare **3** (12.9 mg, 89.2%). ¹H NMR (400 MHz, CDCl₃) δ 8.28 (s, 1H), 8.14 (d, *J* = 1.2 Hz, 2H), 8.02 (d, *J* = 4.4 Hz, 1H), 7.91 (d, *J* = 8.8 Hz, 1H), 2.85 (s, 3H). MS (ESI) *m/z* 298.0 [M+H]⁺.

6-(Tributylstannyl)-2-naphthaldehyde (10). Compound **10** was synthesized from **9** according to the method described above to prepare **2** (119 mg, 62.6%). ¹H NMR (400 MHz, CDCl₃) δ 10.1 (s, 1H), 8.43 (d, *J* = 8.8 Hz, 2H), 8.01 (dd, *J* = 2.0, 8.8 Hz, 1H), 7.90 (dd, *J* = 1.6, 7.6 Hz, 1H), 7.80 (d, *J* = 8.4 Hz, 1H), 7.68 (d, *J* = 8.4 Hz, 1H), 1.76–1.55 (m, 6H), 1.44–1.32 (m, 6H), 1.24–1.10 (m, 6H), 0.92–0.88 (m, 9H). MS (ESI) *m/z* 447.2 [M+H]⁺.

6-Iodo-2-naphthaldehyde (11). Compound **11** was synthesized from **10** according to the method described above to prepare **3** (68.5 mg, 91.2%). ¹H NMR (400 MHz, CDCl₃) δ 10.2 (s, 1H), 8.31 (d, *J* = 9.6 Hz, 2H), 7.97 (dd, *J* = 1.6, 8.4 Hz, 1H), 7.84 (dd, *J* = 2.0, 8.8 Hz, 1H), 7.82 (d, *J* = 8.4 Hz, 1H), 7.73 (d, *J* = 8.8 Hz, 1H). MS (ESI) *m/z* 283.0 [M+H]⁺.

1-(6-Iodonaphthalen-2-yl)ethanone (12). Compound **12** was synthesized from **11** according to the method described above to prepare **6** (15.2 mg, 48.3%). ¹H NMR (400 MHz, CDCl₃) δ 8.24 (s, 1H), 7.78 (d, *J* = 9.2 Hz, 2H), 7.77 (dd, *J* = 1.6, 8.8 Hz, 1H), 7.68 (s, 1H), 7.56 (d, *J* = 8.4 Hz, 1H), 1.81 (s, 3H). MS (ESI) *m/z* 297.0 [M+H]⁺.

6-Bromo-2-methylquinoxaline (14). A mixture of **13** (935 mg, 5.0 mmol) and methylglyoxal (40% in H₂O) (450 μ L, 6.5 mmol) in EtOH (50 mL) was stirred at 50 °C for 10 h. The mixture was concentrated and purified by silica gel chromatography (ethyl acetate/hexane = 1/3) to give **14** (710 mg, 63.6%). ¹H NMR (400 MHz, CDCl₃) δ 8.74 (d, *J* = 1.6 Hz, 1H), 8.23 (dd, *J* = 2.0, 20 Hz, 1H), 7.91 (q, *J* = 9.5 Hz, 1H), 7.80 (ddd, *J* = 2.0, 8.8, 14 Hz, 1H), 2.78 (s, 3H). MS (ESI) *m/z* 223.0 [M+H]⁺.

6-Bromo-2-Quinoxalinecarboxaldehyde (15). Compound **15** was synthesized from **14** according to the method described above to prepare **5** (324 mg, 68.3%). ¹H NMR (400 MHz, CDCl₃) δ 10.3 (s, 1H), 9.42 (d, *J* = 2.0 Hz, 1H), 8.43 (dd, *J* = 2.4, 15.6 Hz, 1H), 8.10 (q, *J* = 7.6 Hz, 1H), 7.99 (ddd, *J* = 2.0, 9.2, 11.3 Hz, 1H). MS (ESI) *m/z* 237.0 [M+H]⁺.

1-(6-Bromoquinoxalin-2-yl)ethanone (16). Compound **16** was synthesized from **15** according to the method described above to prepare **6** (205 mg, 97.0%). ¹H NMR (400 MHz, CDCl₃) δ 8.73 (s, 1H), 8.18 (d, *J* = 2.0 Hz, 1H), 7.92 (d, *J* = 8.8 Hz, 1H), 7.77 (dd, *J* = 2.4, 8.8 Hz, 1H), 2.77 (s, 3H). MS (ESI) *m/z* 251.0 [M+H]⁺.

1-(6-(Tributylstannyl)quinoxalin-2-yl)ethanone (17). Compound 17 was synthesized from 16 according to the method described above to prepare 2 (131 mg, 69.2%). ¹H NMR (400 MHz, CDCl₃) δ 8.72 (s, 1H), 8.15 (s, 1H), 8.01 (d, J = 8.0 Hz, 1H), 7.80 (d, J = 8.4 Hz, 1H), 2.78 (s, 3H), 1.66–1.55 (m, 6H), 1.37–1.34 (m, 6H), 1.18–1.11 (m, 6H), 0.90–0.87 (m, 9H). MS (ESI) *m/z* 463.2 [M+H]⁺.

1-(6-Iodoquinoxalin-2-yl)ethanone (18). Compound 18 was synthesized from 17 according to the method described above to prepare 3 (26.8 mg, 63.4%). ¹H NMR (400 MHz, CDCl₃) δ 8.74 (s, 1H), 8.44 (s, 1H), 7.95 (dd, J = 2.0, 8.8 Hz, 1H), 7.78 (d, J = 8.4 Hz, 1H), 2.77 (s, 3H). MS (ESI) *m/z* 299.0 [M+H]⁺.

(2E)-3-(4-Nitrophenyl)prop-2-enal (20). A mixture of 19 (302 mg, 2.0 mmol), (1,3-dioxolan-2-yl)methyltriphenylphosphonium bromide (1717 mg, 4.0 mmol), 18-crown-6 (catalyst), and NaH (192 mg, 8.0 mmol) in tetrahydrofuran (THF) (30 mL) was stirred for 2 h at rt. HCl aq (6 N, 2.0 mL) was added to hydrolyze the dioxolane function. The mixture was extracted with chloroform after neutralization with 1 N NaOH aq (12 mL), and the combined organic layer was dried over Na₂SO₄, concentrated, and purified by silica gel chromatography (ethyl acetate/hexane = 1/2) to give 20 (184.5 mg, 52.1%). ¹H NMR (400 MHz, CDCl₃) δ 9.78 (d, J = 7.6 Hz, 1H), 8.30 (d, J = 8.8 Hz, 2H), 7.73 (d, J = 8.8 Hz, 2H), 7.53 (d, J = 1.6 Hz, 1H), 6.81 (q, J = 7.9 Hz, 1H).

(2E,4E)-5-(4-Nitrophenyl)penta-2,4-dienal (21). Compound 21 was synthesized from 20 according to the method described above to prepare 20 (146 mg, 51.6%). ¹H NMR (400 MHz, CDCl₃) δ 9.68 (d, J = 7.6 Hz, 1H), 8.25 (d, J = 8.8 Hz, 2H), 7.65 (d, J = 8.8 Hz, 2H), 7.31–7.25 (m, 1H), 7.17–7.03 (m, 2H), 6.37 (q, J = 7.7 Hz, 1H).

(2E,4E,6E)-7-(4-(Dimethylamino)phenyl)-1-(2-iodopyridinyl)hepta-2,4,6-trien-1-one (22, PYDP-3). To a solution of (2E,4E)-5-(4-(dimethylamino)phenyl)penta-2,4-dienal (14.0 mg, 0.070 mmol) in a mixed solvent (4 mL, 4: 1 EtOH/DMF mixture) was added 3 (17.1 mg, 0.070 mmol). The mixture was stirred at 0 °C for 10 min. Then, 1.5 mL of 10% KOH aq was added in a dropwise manner to the reaction mixture. The mixture was stirred at rt for 8 h, extracted with chloroform, and the combined organic layer was dried over Na₂SO₄, concentrated, and purified by silica gel chromatography (ethyl acetate/hexane = 1/2) to give 4.1 mg of 22 (13.6%). ¹H NMR (400 MHz, CDCl₃) δ 8.89 (d, J = 2.4 Hz, 1H), 8.21 (d, J = 8.8 Hz, 2H), 7.82 (d, J = 8.8 Hz, 1H), 7.80 (dd, J = 2.4, 8.4 Hz, 1H), 7.58 (d, J = 11.2 Hz, 2H), 7.55 (dd, J = 2.0, 7.6 Hz, 1H), 7.10 (q, J = 8.8 Hz, 1H), 6.92–6.80 (m, 3H), 6.74 (dd, J = 9.2, 14.8 Hz, 1H), 3.01 (s, 6H). MS (EI) *m/z* 430.1 [M]⁺.

(2E,4E,6E)-7-(4-(Dimethylamino)phenyl)-1-(6-iodoquinolinyl)hepta-2,4,6-trien-1-one (23, QLDP-3). Compound 23 was synthesized from 8 and 21 according to the method described above to prepare 22 (8.0 mg, 49.5%). ¹H NMR (400 MHz, CDCl₃) δ 8.28 (d, J = 1.6 Hz, 1H), 8.25 (d, J = 8.8 Hz, 1H), 8.16 (d, J = 8.8 Hz, 1H), 8.02 (dd, J = 2.0, 8.8 Hz, 1H), 7.95 (d, J = 8.8 Hz, 1H), 7.86 (d, J = 15.2 Hz, 1H), 7.73 (dd, J = 11.2, 15.2 Hz, 1H), 7.37 (d, J = 8.8 Hz, 2H), 6.92 (q, J = 7.9 Hz, 1H), 6.78 (d, J = 8.8 Hz, 1H), 6.73–6.67 (m, 3H), 6.66–6.59 (m, 1H), 3.01 (s, 6H). MS (EI) *m/z* 480.1 [M]⁺.

(2E,4E,6E)-7-(4-(Dimethylamino)phenyl)-1-(6-iodonaphthyl)hepta-2,4,6-trien-1-one (24, NPDP-3). Compound 24 was synthesized from 12 and 21 according to the method described above to prepare 22 (1.7 mg, 12.3%). ¹H NMR (400 MHz, CDCl₃) δ 9.56 (d, J = 8.4 Hz, 1H), 7.74 (d, J = 8.4 Hz, 2H), 7.32 (dd, J = 3.2, 9.6 Hz, 2H), 6.72–6.65 (m, 6H), 6.61–6.52 (m, 2H), 6.48–6.31 (m, 2H), 6.14 (q, J = 7.7 Hz, 1H), 3.10 (s, 6H). MS (EI) *m/z* 479.1 [M]⁺.

(2E,4E,6E)-7-(4-(Dimethylamino)phenyl)-1-(6-iodoquinoxalinyl)hepta-2,4,6-trien-1-one (25, QXDP-3). Compound 25 was synthesized from 18 and 21 according to the method described above to prepare 22 (1.8 mg, 8.4%). ¹H NMR (400 MHz, CDCl₃) δ 9.58 (d, J = 6.8 Hz, 1H), 8.64 (d, J = 24.4 Hz, 1H), 8.10 (d, J = 8.4 Hz, 1H), 7.89 (dd, J = 4.0, 8.8 Hz, 1H), 7.76 (d, J = 12.0 Hz, 1H), 7.72 (d, J = 10.0 Hz, 1H), 7.38 (d, J = 7.2 Hz, 2H), 7.00–6.94 (m, 1H), 6.81–6.78 (m, 2H), 6.69 (d, J = 8.0 Hz, 2H), 6.61 (dd, J = 11.2, 14 Hz, 1H), 3.02 (s, 6H). MS (EI) *m/z* 481.1 [M]⁺.

(2E,4E,6E)-7-(4-Nitrophenyl)-1-(2-iodopyridinyl)hepta-2,4,6-trien-1-one (26, PYNP-3). Compound 26 was synthesized from 3

and 21 according to the method described above to prepare 22 (1.4 mg, 9.4%). ¹H NMR (400 MHz, CDCl₃) δ 8.88 (d, J = 2.0 Hz, 1H), 8.22 (d, J = 8.8 Hz, 2H), 7.89 (d, J = 8.0 Hz, 1H), 7.85 (dd, J = 2.4, 8.4 Hz, 1H), 7.59 (d, J = 9.2 Hz, 2H), 7.58 (dd, J = 4.0, 9.2 Hz, 1H), 7.06 (q, J = 8.8 Hz, 1H), 6.99–6.83 (m, 3H), 6.70 (dd, J = 11.2, 14.8 Hz, 1H). MS (EI) *m/z* 432.0 [M]⁺.

(2E,4E,6E)-7-(4-Nitrophenyl)-1-(6-iodoquinolinyl)hepta-2,4,6-trien-1-one (27, QLNP-3). Compound 27 was synthesized from 8 and 21 according to the method described above to prepare 22 (0.90 mg, 17.0%). ¹H NMR (400 MHz, CDCl₃) δ 8.31 (d, J = 2.0 Hz, 1H), 8.26 (d, J = 8.8 Hz, 1H), 8.17 (d, J = 8.4 Hz, 1H), 7.99 (dd, J = 1.6, 8.0 Hz, 1H), 7.92 (d, J = 7.6 Hz, 1H), 7.87 (d, J = 9.2 Hz, 1H), 7.68 (dd, J = 9.2, 14.0 Hz, 1H), 7.30 (d, J = 8.4 Hz, 2H), 6.88 (q, J = 7.9 Hz, 1H), 6.72 (d, J = 2.4 Hz, 1H), 6.68–6.60 (m, 3H), 6.60–6.56 (m, 1H). MS (EI) *m/z* 482.0 [M]⁺.

(2E,4E,6E)-7-(4-Nitrophenyl)-1-(6-iodonaphthyl)hepta-2,4,6-trien-1-one (28, NPNP-3). Compound 28 was synthesized from 12 and 21 according to the method described above to prepare 22 (0.60 mg, 4.6%). ¹H NMR (400 MHz, CDCl₃) δ 9.52 (d, J = 7.2 Hz, 1H), 7.80 (d, J = 8.4 Hz, 2H), 7.38 (dd, J = 4.0, 8.8 Hz, 2H), 6.70–6.63 (m, 6H), 6.55–6.51 (m, 2H), 6.38–6.30 (m, 2H), 6.22 (q, J = 7.9 Hz, 1H). MS (EI) *m/z* 481.0 [M]⁺.

(2E,4E,6E)-7-(4-Nitrophenyl)-1-(6-iodoquinoxalinyl)hepta-2,4,6-trien-1-one (29, QXNP-3). Compound 29 was synthesized from 18 and 21 according to the method described above to prepare 22 (1.3 mg, 9.9%). ¹H NMR (400 MHz, CDCl₃) δ 9.57 (d, J = 5.6 Hz, 1H), 8.60 (d, J = 12.0 Hz, 1H), 8.02 (d, J = 8.8 Hz, 1H), 7.82 (dd, J = 2.4, 8.0 Hz, 1H), 7.70 (d, J = 9.2 Hz, 1H), 7.68 (d, J = 8.0 Hz, 1H), 7.36 (d, J = 8.4 Hz, 2H), 7.02–6.94 (m, 1H), 6.79–6.76 (m, 2H), 6.66 (d, J = 8.8 Hz, 2H), 6.48 (dd, J = 4.0, 8.8 Hz, 1H). MS (EI) *m/z* 483.0 [M]⁺.

(2E,4E,6E)-7-(4-Nitrophenyl)-1-(4-iodophenyl)hepta-2,4,6-trien-1-one (30, PHNP-3). Compound 30 was synthesized from 21 and 4-iodoacetophenone according to the method described above to prepare 22 (6.7 mg, 39.0%). ¹H NMR (400 MHz, CDCl₃) δ 8.21 (d, J = 8.4 Hz, 2H), 7.86 (d, J = 8.4 Hz, 2H), 7.69 (d, J = 8.8 Hz, 2H), 7.58 (d, J = 8.4 Hz, 2H), 7.52 (q, J = 4.9 Hz, 1H), 7.09–7.01 (m, 2H), 6.91–6.80 (m, 2H), 6.68 (dd, J = 11.2, 14.0 Hz, 1H). MS (EI) *m/z* 431.0 [M]⁺.

(2E,4E,6E)-7-(4-Nitrophenyl)-1-(4-bromophenyl)hepta-2,4,6-trien-1-one (31). Compound 31 was synthesized from 21 and 4-iodoacetophenone according to the method described above to prepare 22 (26.8 mg, 65.1%). ¹H NMR (400 MHz, CDCl₃) δ 8.21 (d, J = 8.4 Hz, 2H), 7.84 (d, J = 8.0 Hz, 2H), 7.64 (d, J = 7.6 Hz, 2H), 7.58 (d, J = 8.8 Hz, 2H), 7.53 (dd, J = 3.6, 10.8 Hz, 1H), 7.04 (dd, J = 3.2, 14.8 Hz, 2H), 6.85 (q, J = 13.6 Hz, 2H), 6.69 (dd, J = 10.8, 14.8 Hz, 1H). MS (ESI) *m/z* 384.1 [M+H]⁺.

(2E,4E,6E)-7-(4-Nitrophenyl)-1-(4-(tributylstannyl)phenyl)hepta-2,4,6-trien-1-one (32). Compound 32 was synthesized from 31 according to the method described above to prepare 2 (6.0 mg, 14.4%). ¹H NMR (400 MHz, CDCl₃) δ 8.22 (d, J = 1.6 Hz, 2H), 7.89 (d, J = 8.0 Hz, 2H), 7.61 (d, J = 8.0 Hz, 2H), 7.58 (d, J = 8.8 Hz, 2H), 7.52 (dd, J = 3.6, 11.6 Hz, 1H), 7.10 (d, J = 14.8 Hz, 1H), 7.06 (q, J = 8.8 Hz, 1H), 6.83 (q, J = 13.6 Hz, 2H), 6.72 (dd, J = 3.2, 14.4 Hz, 1H), 1.56–1.53 (m, 6H), 1.36–1.31 (m, 6H), 1.16–1.01 (m, 6H), 0.91–0.87 (m, 9H). MS (ESI) *m/z* 596.4 [M+H]⁺.

Competitive Inhibition Assay. This experiment was conducted based on our method reported previously.³² In this assay, the half maximal inhibitory concentration (IC₅₀) and K_i values were calculated when % control decreased more than 50% dependent on the concentration of test compounds. Otherwise, IC₅₀ and K_i were not determined (referred to as “n.d.”).

Fluorescence Staining. This experiment was conducted based on our method reported previously. Brain sections were incubated with a 50% EtOH solution of each chalcone analogue (30 μM) for 30 min. Fluorescent staining results were acquired on a fluorescence microscope (FSX100, Olympus Corp., Tokyo, Japan) equipped with a U-MWIG3 filter set.

Immunohistochemical Staining. This experiment was conducted based on our method reported previously. Brain sections were

incubated with a goat anti-mouse IgG (Histofine Simple Stain Mouse MAX-PO (MULTI), Nichirei Biosciences Inc., Tokyo, Japan) at rt for 30 min after incubation with anti-phosphorylated α -syn or anti-A β primary antibodies followed by rinsing in PBS-Tween20. After three 3 min rinses in PBS-Tween 20 and one 5 min rinse in TBS, the sections were incubated with 3,3'-diaminobenzidine as a chromogen for 1 min. After being washed with H₂O, the sections were observed using a microscope (FSX100, Olympus Corp.).

¹²⁵I-Labeling Reaction. This experiment was conducted based on our method reported previously.³⁰ In this experiment, to a mixture of [¹²⁵I]NaI (3.70 MBq, specific activity: 81.4 TBq/mmol) in 50 μ L DMF, 100 μ L of 3% H₂O₂ aq, and 100 μ L of 1 N HCl aq in a sealed vial was added a tributyltin precursor, 32 (200 μ g/200 μ L EtOH). The reaction was left at 80 °C for 5 min.

Biodistribution Study. This experiment was conducted based on our method reported previously.³² [¹²⁵I]PHNP-3 (18.5 kBq in 100 μ L) was injected in this experiment.

■ ASSOCIATED CONTENT

SI Supporting Information

The Supporting Information is available free of charge at <https://pubs.acs.org/doi/10.1021/acschemneuro.1c00441>.

Results of the fluorescent staining, binding saturation assay, and in vitro analysis of stability in murine plasma (PDF)

■ AUTHOR INFORMATION

Corresponding Author

Masahiro Ono – Department of Patho-Functional Bioanalysis, Graduate School of Pharmaceutical Sciences, Kyoto University, Kyoto 606-8501, Japan; orcid.org/0000-0002-2497-039X; Phone: +81-75-753-4556; Email: ono@pharm.kyoto-u.ac.jp; Fax: +81-75-753-4568

Authors

Sho Kaide – Department of Patho-Functional Bioanalysis, Graduate School of Pharmaceutical Sciences, Kyoto University, Kyoto 606-8501, Japan

Hiroyuki Watanabe – Department of Patho-Functional Bioanalysis, Graduate School of Pharmaceutical Sciences, Kyoto University, Kyoto 606-8501, Japan; orcid.org/0000-0002-8873-1224

Shimpei Iikuni – Department of Patho-Functional Bioanalysis, Graduate School of Pharmaceutical Sciences, Kyoto University, Kyoto 606-8501, Japan; orcid.org/0000-0002-7073-9084

Masato Hasegawa – Department of Brain and Neurosciences, Tokyo Metropolitan Institute of Medical Science, Tokyo 156-8506, Japan

Kyoko Itoh – Department of Pathology & Applied Neurobiology, Kyoto Prefectural University of Medicine, Graduate School of Medical Science, Kyoto 602-8566, Japan

Complete contact information is available at:

<https://pubs.acs.org/doi/10.1021/acschemneuro.1c00441>

Author Contributions

S.K. and H.W. designed the study, executed in vitro and in vivo experiments, interpreted the results, and wrote the manuscript. M.H. assisted with studies using α -syn aggregates. K.I. assisted with studies using postmortem human brain samples. S.K., H.W., S.I., and M.O. reviewed the manuscript. M.O. conceived, designed, and supervised this project. All authors have given approval to the final version of the manuscript.

Funding

This research was supported by the Naito Foundation and JSPS KAKENHI grant numbers 20J14694 and 20H03622.

Notes

The authors declare no competing financial interest.

■ ABBREVIATIONS

α -syn, α -synuclein; AD, Alzheimer's disease; A β , amyloid β ; ARG, autoradiography; (Bu₃Sn)₂, bis(tributyltin); BBB, blood–brain barrier; DMF, *N,N*-dimethylformamide; HPLC, high-performance liquid chromatography; PD, Parkinson's disease; % ID/g, percentage injected dose per gram; PBS, phosphate-buffered saline; PET, positron emission tomography; SPECT, single-photon emission computed tomography; THF, tetrahydrofuran; Pd(PPh₃)₄, tetrakis-(triphenylphosphine)palladium(0); ThT, thioflavin T; Et₃N, triethylamine; TBS, Tris-buffered saline

■ REFERENCES

- (1) Spillantini, M. G.; Schmidt, M. L.; Lee, V. M.-Y.; Trojanowski, J. Q.; Jakes, R.; Goedert, M. α -Synuclein in Lewy bodies. *Nature* **1997**, *388*, 839–840.
- (2) Spillantini, M. G.; Crowther, R. A.; Jakes, R.; Cairns, N. J.; Lantos, P. L.; Goedert, M. Filamentous α -synuclein inclusions link multiple system atrophy with Parkinson's disease and dementia with Lewy bodies. *Neurosci. Lett.* **1998**, *251*, 205–208.
- (3) Tu, P.-H.; Galvin, J. E.; Baba, M.; Giasson, B.; Tomita, T.; Leight, S.; Nakajo, S.; Iwatsubo, T.; Trojanowski, J. Q.; Lee, V. M.-Y. Glial cytoplasmic inclusions in white matter oligodendrocytes of multiple system atrophy brains contain insoluble α -synuclein. *Ann. Neurol.* **1998**, *44*, 415–422.
- (4) Wakabayashi, K.; Yoshimoto, M.; Tsuji, S.; Takahashi, H. α -Synuclein immunoreactivity in glial cytoplasmic inclusions in multiple system atrophy. *Neurosci. Lett.* **1998**, *249*, 180–182.
- (5) Irwin, D. J.; Lee, V. M.-Y.; Trojanowski, J. Q. Parkinson's disease dementia: convergence of α -synuclein, tau and amyloid- β pathologies. *Nat. Rev. Neurosci.* **2013**, *14*, 626–636.
- (6) Goedert, M.; Jakes, R.; Spillantini, M. G. The Synucleinopathies: Twenty Years On. *J. Parkinsons. Dis.* **2017**, *7*, S51–S69.
- (7) Seidel, K.; Mahlke, J.; Siswanto, S.; Krüger, R.; Heinsen, H.; Auburger, G.; Bouzrou, M.; Grinberg, L. T.; Wicht, H.; Korff, H. W.; den Dunnen, W.; Rüb, U. The Brainstem Pathologies of Parkinson's Disease and Dementia With Lewy Bodies. *Brain Pathol.* **2015**, *25*, 121–135.
- (8) Yamasaki, T. R.; Holmes, B. B.; Furman, J. L.; Dhavale, D. D.; Su, B. W.; Song, E. S.; Cairns, N. J.; Kotzbauer, P. T.; Diamond, M. I. Parkinson's disease and multiple system atrophy have distinct α -synuclein seed characteristics. *J. Biol. Chem.* **2019**, *294*, 1045–1058.
- (9) Eberling, J. L.; Dave, K. D.; Frasier, M. A. α -Synuclein imaging: a critical need for Parkinson's disease research. *J. Parkinsons. Dis.* **2013**, *3*, 565–567.
- (10) Shah, M.; Seibyl, J.; Cartier, A.; Bhatt, R.; Catafau, A. M. Molecular imaging insights into neurodegeneration: focus on α -synuclein radiotracers. *J. Nucl. Med.* **2014**, *55*, 1397–1400.
- (11) Miranda-Azpiazu, P.; Svedberg, M.; Higuchi, M.; Ono, M.; Jia, Z.; Sunnemark, D.; Elmore, C. S.; Schou, M.; Varrone, A. Identification and in vitro characterization of C05-01, a PBB3 derivative with improved affinity for alpha-synuclein. *Brain Res.* **2020**, *1749*, 147131.
- (12) Kotzbauer, P. T.; Cairns, N. J.; Campbell, M. C.; Willis, A. W.; Racette, B. A.; Tabbal, S. D.; Perlmutter, J. S. Pathologic accumulation of α -synuclein and A β in Parkinson disease patients with dementia. *Arch. Neurol.* **2012**, *69*, 1326–1331.
- (13) Villemagne, V. L.; Fodero-Tavoletti, M. T.; Masters, C. L.; Rowe, C. C. Tau imaging: early progress and future directions. *Lancet Neurol.* **2015**, *14*, 114–124.

- (14) Xu, M. M.; Ryan, P.; Rudrawar, S.; Quinn, R. J.; Zhang, H. Y.; Mellick, G. D. Advances in the development of imaging probes and aggregation inhibitors for α -synuclein. *Acta Pharmacol. Sin.* **2020**, *41*, 483–498.
- (15) Villemagne, V. L.; Doré, V.; Burnham, S. C.; Masters, C. L.; Rowe, C. C. Imaging tau and amyloid- β proteinopathies in Alzheimer disease and other conditions. *Nat. Rev. Neurol.* **2018**, *14*, 225–236.
- (16) Leuzy, A.; Chiotis, K.; Lemoine, L.; Gillberg, P. G.; Almkvist, O.; Rodriguez-Vieitez, E.; Nordberg, A. Tau PET imaging in neurodegenerative tauopathies-still a challenge. *Mol. Psychiatry* **2019**, *24*, 1112–1134.
- (17) Fodero-Tavoletti, M. T.; Mulligan, R. S.; Okamura, N.; Furumoto, S.; Rowe, C. C.; Kudo, Y.; Masters, C. L.; Cappai, R.; Yanai, K.; Villemagne, V. L. In vitro characterisation of BF227 binding to α -synuclein/Lewy bodies. *Eur. J. Pharmacol.* **2009**, *617*, 54–58.
- (18) Yu, L.; Cui, J.; Padakanti, P. K.; Engel, L.; Bagchi, D. P.; Kotzbauer, P. T.; Tu, Z. Synthesis and in vitro evaluation of α -synuclein ligands. *Bioorg. Med. Chem.* **2012**, *20*, 4625–4634.
- (19) Bagchi, D. P.; Yu, L.; Perlmutter, J. S.; Xu, J.; Mach, R. H.; Tu, Z.; Kotzbauer, P. T. Binding of the radioligand SIL23 to α -synuclein fibrils in Parkinson disease brain tissue establishes feasibility and screening approaches for developing a Parkinson disease imaging agent. *PLoS One* **2013**, *8*, No. e55031.
- (20) Zhang, X.; Jin, H.; Padakanti, P.; Li, J.; Yang, H.; Fan, J.; Mach, R.; Kotzbauer, P.; Tu, Z. Radiosynthesis and in Vivo Evaluation of Two PET Radioligands for Imaging α -Synuclein. *Appl. Sci.* **2014**, *4*, 66–78.
- (21) Chu, W.; Zhou, D.; Gaba, V.; Liu, J.; Li, S.; Peng, X.; Xu, J.; Dhavale, D.; Bagchi, D. P.; d'Avignon, A.; Shakerdge, N. B.; Bacskai, B. J.; Tu, Z.; Kotzbauer, P. T.; Mach, R. H. Design, Synthesis, and Characterization of 3-(Benzylidene)indolin-2-one Derivatives as Ligands for α -Synuclein Fibrils. *J. Med. Chem.* **2015**, *58*, 6002–6017.
- (22) Mathis, C. A.; Lopresti, B. J.; Ikonovic, M. D.; Klunk, W. E. Small-molecule PET Tracers for Imaging Proteinopathies. *Semin. Nucl. Med.* **2017**, *47*, 553–575.
- (23) Hsieh, C. J.; Ferrie, J. J.; Xu, K.; Lee, I.; Graham, T. J. A.; Tu, Z.; Yu, J.; Dhavale, D.; Kotzbauer, P.; Petersson, E. J.; Mach, R. H. Alpha Synuclein Fibrils Contain Multiple Binding Sites for Small Molecules. *ACS Chem. Neurosci.* **2018**, *9*, 2521–2527.
- (24) Bousset, L.; Pieri, L.; Ruiz-Arlandis, G.; Gath, J.; Jensen, P. H.; Habenstein, B.; Madiona, K.; Olieric, V.; Böckmann, A.; Meier, B. H.; Melki, R. Structural and functional characterization of two alpha-synuclein strains. *Nat. Commun.* **2013**, *4*, 2575.
- (25) Li, B.; Ge, P.; Murray, K. A.; Sheth, P.; Zhang, M.; Nair, G.; Sawaya, M. R.; Shin, W. S.; Boyer, D. R.; Ye, S.; Eisenberg, D. S.; Zhou, Z. H.; Jiang, L. Cryo-EM of full-length α -synuclein reveals fibril polymorphs with a common structural kernel. *Nat. Commun.* **2018**, *9*, 3609.
- (26) Peng, C.; Gathagan, R. J.; Covell, D. J.; Medellin, C.; Stieber, A.; Robinson, J. L.; Zhang, B.; Pitkin, R. M.; Olufemi, F. M.; Luk, K. C.; Trojanowski, J. Q.; Lee, V. M.-Y. Cellular milieu imparts distinct pathological α -synuclein strains in α -synucleinopathies. *Nature* **2018**, *557*, 558–563.
- (27) Verduran, M.; Levigoureux, E.; Zeinyeh, W.; Berthier, L.; Mendjel-Herda, M.; Cadarossanesaib, F.; Bouillot, C.; Iecker, T.; Terreux, R.; Lancelot, S.; Chauveau, F.; Billard, T.; Zimmer, L. In Silico, in Vitro, and in Vivo Evaluation of New Candidates for α -Synuclein PET Imaging. *Mol. Pharmaceutics* **2018**, *15*, 3153–3166.
- (28) Ferrie, J. J.; Lengyel-Zhand, Z.; Janssen, B.; Lougee, M. G.; Giannakoulas, S.; Hsieh, C.-J.; Pagar, V. V.; Weng, C.-C.; Xu, H.; Graham, T. J. A.; Lee, V. M.-Y.; Mach, R. H.; Petersson, E. J. Identification of a nanomolar affinity α -synuclein fibril imaging probe by ultra-high throughput in silico screening. *Chem. Sci.* **2020**, *11*, 12746–12754.
- (29) Kuebler, L.; Buss, S.; Leonov, A.; Ryazanov, S.; Schmidt, F.; Maurer, A.; Weckbecker, D.; Landau, A. M.; Lillethorup, T. P.; Bleher, D.; Saw, R. S.; Pichler, B. J.; Griesinger, C.; Giese, A.; Herfert, K. [^{11}C]MODAG-001-towards a PET tracer targeting α -synuclein aggregates. *Eur. J. Nucl. Med. Mol. Imaging* **2021**, *48*, 1759–1772.
- (30) Ono, M.; Doi, Y.; Watanabe, H.; Ihara, M.; Ozaki, A.; Saji, H. Structure-activity relationships of radioiodinated diphenyl derivatives with different conjugated double bonds as ligands for α -synuclein aggregates. *RSC Adv.* **2016**, *6*, 44305–44312.
- (31) Watanabe, H.; Ariyoshi, T.; Ozaki, A.; Ihara, M.; Ono, M.; Saji, H. Synthesis and biological evaluation of novel radioiodinated benzimidazole derivatives for imaging α -synuclein aggregates. *Bioorg. Med. Chem.* **2017**, *25*, 6398–6403.
- (32) Kaide, S.; Watanabe, H.; Shimizu, Y.; Iikuni, S.; Nakamoto, Y.; Hasegawa, M.; Itoh, K.; Ono, M. Identification and Evaluation of Bisquinoline Scaffold as a New Candidate for α -Synuclein-PET Imaging. *ACS Chem. Neurosci.* **2020**, *11*, 4254–4261.
- (33) Thapa, P.; Upadhyay, S. P.; Suo, W. Z.; Singh, V.; Gurung, P.; Lee, E. S.; Sharma, R.; Sharma, M. Chalcone and its analogs: Therapeutic and diagnostic applications in Alzheimer's disease. *Bioorg. Chem.* **2021**, *108*, 104681.
- (34) Ono, M.; Hori, M.; Haratake, M.; Tomiyama, T.; Mori, H.; Nakayama, M. Structure-activity relationship of chalcones and related derivatives as ligands for detecting of β -amyloid plaques in the brain. *Bioorg. Med. Chem.* **2007**, *15*, 6388–6396.
- (35) LeVine, H., III Thioflavine T interaction with synthetic Alzheimer's disease β -amyloid peptides: detection of amyloid aggregation in solution. *Protein Sci.* **1993**, *2*, 404–410.
- (36) Cui, M.; Ono, M.; Kimura, H.; Liu, B. L.; Saji, H. Synthesis and biological evaluation of indole-chalcone derivatives as β -amyloid imaging probe. *Bioorg. Med. Chem. Lett.* **2011**, *21*, 980–982.
- (37) Lengyel-Zhand, Z.; Ferrie, J. J.; Janssen, B.; Hsieh, C.-J.; Graham, T.; Xu, K.-Y.; Haney, C. M.; Lee, V. M.-Y.; Trojanowski, J. Q.; Petersson, E. J.; Mach, R. H. Synthesis and characterization of high affinity fluorogenic α -synuclein probes. *Chem. Commun.* **2020**, *56*, 3567–3570.
- (38) Ono, M.; Takahashi, M.; Shimozaawa, A.; Fujinaga, M.; Mori, W.; Nagai, Y.; Mimura, K.; Minamihisamatsu, T.; Uchida, S.; Kumata, K.; Shimojo, M.; Takado, Y.; Takuwa, H.; Shimizu, H.; Kakita, A.; Sahara, N.; Zhang, M.-R.; Minaminoto, T.; Hasegawa, M.; Higuchi, M. In vivo visualization of propagating α -synuclein pathologies in mouse and marmoset models by a bimodal imaging probe, C05-05. *bioRxiv*. 349860. 2020.
- (39) Dishino, D. D.; Welch, M. J.; Kilbourn, M. R.; Raichle, M. E. Relationship between lipophilicity and brain extraction of C-11-labeled radiopharmaceuticals. *J. Nucl. Med.* **1983**, *24*, 1030–1038.
- (40) Okamura, N.; Harada, R.; Furumoto, S.; Arai, H.; Yanai, K.; Kudo, Y. Tau PET imaging in Alzheimer's disease. *Curr. Neurol. Neurosci. Rep.* **2014**, *14*, 500.
- (41) Harada, R.; Okamura, N.; Furumoto, S.; Yanai, K. Imaging Protein Misfolding in the Brain Using β -Sheet Ligands. *Front. Neurosci.* **2018**, *12*, 585.